Chemical Engineering Science: X 8 (2020) 100078

Contents lists available at ScienceDirect

Chemical Engineering Science: X

journal homepage: www.elsevier.com/locate/cesx

Synthesis of grid compliant substitute natural gas from a representative biogas mixture in a hybrid Ni/Ru catalysed reactor

Emanuele Moioli [a,b,*,1,2], Robin Mutschler [a,b,1], Alexandre Borsay [a,b,1], Marco Calizzi [a,b], Andreas Züttel [a,b]

[a] Laboratory of Materials for Renewable Energy (LMER), Institute of Chemical Sciences and Engineering (ISIC), Basic Science Faculty (SB), École Polytechnique Fédérale de Lausanne (EPFL) Valais/Wallis, Energypolis, Sion, Switzerland
[b] Empa Materials Science & Technology, Dübendorf, Switzerland

ARTICLE INFO

Article history:
Received 8 August 2020
Received in revised form 2 September 2020
Accepted 8 September 2020

Keywords:
CO_2 methanation
Multistep reactor
Optimal temperature profile
Biogas upgrading

ABSTRACT

We demonstrate biogas upgrading towards full CO_2 conversion in mild conditions in a three-step reactor system using Ru- and Ni-based catalysts. In each of the three reactor stages, the temperature is carefully controlled, thus optimizing the reaction thermodynamics and kinetics, resulting in a maximized global CO_2 conversion. At ambient pressure, 92% conversion can be achieved over a commercial Ru/Al_2O_3 catalyst at a space velocity of 2 $L/h/g_{cat}$ in every stage. At 2 bar conversion is enhanced to above 99%. It is possible to substitute the Ru-based catalyst in the first stage with a cheaper Ni-based catalyst, shifting the first-stage temperature to higher values forming also CO. CO has a positive effect on the following step since CO is converted to CH_4 in the CO methanation reaction. In this way, it is possible to achieve the same final conversion compared to the Ru-operated reactor system using Ni in the first reactor stage.

1. Introduction

Power to gas (PtG) and biomethane production are two promising concepts for the development of the renewable energy based economy. However, their development is currently slowed by concurrent problems. PtG requires CO_2 as a carbon source and no technology nowadays provides this compound at a competitive price and in a reliable way (Götz et al., 2016). Biogas is a mixture of mainly CH_4 and CO_2 and an expensive (membrane- or scrubber-based) separation of CO_2 must be performed to make it suitable for injection in the natural gas grid, producing biomethane (Kapoor et al. 2019, Witte et al., 2018a). Combining the two concepts is a promising solution because the CO_2 methanation reactor can operate as a unit for biomethane production, CO_2 separation and product gas drying. On the other side, the biogas plant works as a reliable CO_2 source for the PtG system, avoiding uncertainty on the availability of this reactant. By coupling PtG and biogas upgrading, it is possible to operate the storage of renewable energy by the use of flexible units, which are able to operate in dynamic conditions (Jürgensen et al., 2015, 2014).

The process is performed in the so-called Sabatier reactor, where two main reactions take place: the Sabatier reaction (Eq. (1)) and the reverse water gas shift reaction (Eq. (2)).

$$CO_2 + 4H_2 \leftrightarrow CH_4 + 2H_2O \Delta H_0^R = -165 kJ/mol \quad (1)$$

$$CO_2 + H_2 \leftrightarrow CO + H_2O \Delta H_0^R = +41 kJ/mol \quad (2)$$

The produced CO can further react to CH_4 in the CO methanation reaction (Eq. (3), a linear combination of Eqs. (1) and (2)).

$$CO + 3H_2 \leftrightarrow CH_4 + H_2O \Delta H_0^R = -206 kJ/mol \quad (3)$$

The requirements for gas grid injection are strict in terms of CO_2, H_2 and H_2O concentrations. For example, in Switzerland, the highest allowed CO_2 and H_2 concentrations are 2% and 6%, respectively (Schweizerischer Verein des Gas- und Wasserfaches SVGW/SSIGE, 2014, 2013). This means that the CO_2 conversion required is above 99.5%. This conversion level can be reached only at temperatures below 300 °C for pressure up to 10 bar due to thermodynamic limitations (Moioli et al., 2019a). For this reason, the Sabatier reactor must be operated either with a highly-active noble metal-based catalyst (such as Ru) or on a transition metal catalyst with intermediate condensation (Moioli and Züttel, 2020; Mutschler et al., 2018b; Witte et al., 2019).

Because both Sabatier and CO methanation reactions are strongly exothermic, appropriate heat management is required in a Sabatier reactor (Moioli, et al. 2019b). Several approaches are

* Corresponding author at: Rue de l'industrie 17, CH-1950 Sion, Switzerland.
E-mail address: emoioli08@gmail.com (E. Moioli).
[1] These authors equally contributed to the paper.
[2] Present address: Thermochemical processes group, Energy and environment section, Paul Scherrer Institute, Forschungstrasse 111, CH-5232, Villigen, Switzerland.

https://doi.org/10.1016/j.cesx.2020.100078
2590-1400/

possible to handle the problem. Among others, the most studied reactor types for this application are adiabatic reactors with intermediate cooling (De Saint Jean et al., 2015; Schaaf et al., 2014), externally cooled reactors (El Sibai et al., 2017; Jürgensen et al., 2014; Kiewidt and Thöming, 2015) and fluidized bed reactors (Witte et al., 2018b). However, the highest optimization potential for the Sabatier reaction is achievable with the employment of a cooling strategy that is capable of efficiently removing the heat produced, maximizing the reaction rate along the axial coordinate of the reactor (Moioli et al. 2019b). The direct methanation of biogas shows a lower temperature increase than the pure CO_2 hydrogenation reaction, due to the presence of excess methane, which operates as a thermal diluent. However, heat management remains an important factor for the optimization of the reaction. For this reason, we manufactured a new system that is composed of three connected reactors, in which the temperature can be adjusted freely and independently. We experimentally demonstrated that tailoring the temperature in the three reactors, so that the profile results are strictly decreasing, is the key to obtain an important improvement in the CO_2 conversion. This effect can be observed independently from the catalyst used, as it is mainly determined by reaction thermodynamics and thermal management. The first reactor performs most of the reaction, up to the reach of thermodynamic equilibrium. The following reactors provide the residence time to convert the remaining CO_2, finding a matching point between thermodynamics and reaction kinetics.

For what concerns the catalyst employed, the use of a cheap Ni-based catalyst would be highly desirable, but the maximum CO_2 conversion attainable on this type of system is below 90% (Koschany et al., 2016). On the other hand, Ru-based catalysts are reported to be active at the low temperature allowing for the desired 99.5% CO_2 conversion value (Falbo et al., 2018; Gallandat et al., 2018). With the system here presented, we experimentally evaluated the possibility of combining the two catalysts to minimize the amount of Ru required. Furthermore, we tailored the combination of the two catalysts to maximize the reaction rate thanks to the amalgamation of CO and CO_2 methanation because CO is produced at high temperature. We demonstrate that with such a special system, it is possible to produce a gas-grid compliant product already at a pressure of 2 bar.

2. Materials and methods

2.1. Catalysts

For the experiments, a commercial 0.5% Ru/Al_2O_3 catalyst (Sigma-Aldrich) and a Ni metal powder (Goodfellow) were employed. The catalysts were analysed by means of X-ray photoelectron spectroscopy (XPS) and no impurities were found other than oxygen and carbon on the surface. X-ray diffraction (XRD) confirmed the results from XPS. Transmission electron microscopy analysis on the 0.5% Ru/Al_2O_3 catalyst demonstrated that the average particle size is 11.5 nm (Mutschler et al., 2019). To avoid sintering of the Ni powder, the catalyst grains (ca. 1 mm diameter) have been mixed with an equal weight ratio of glass beads (Schäfer glass) with an approximate diameter of 1–1.5 mm. This reduces the thermal stress on the Ni catalyst and prevents evident deactivation phenomena. The glass beads are made of borosilicate and do not show any signs of melting at the maximum temperature of the experiments.

2.2. Reactor

The reactor is composed of three separate cells with an internal diameter of 6 mm. The three cells are heated independently by heating cartridges (Maxiwatt, Spain) placed below the reactive channel. The temperature can be set between 30 and 550 °C. This is below the Tammann temperature of nickel (Fukuhara et al., 2017). The reactor body is included in an insulating foam concrete jacket. The gases are fed through three mass flow controllers (Bronkhorst El Flow series). Between the reactors, connections of 3 mm diameter link the different cells from outside the insulation. These lines are heated at 180 °C. At the reactor outlet, a capillary connected to the mass spectrometer (MS) is installed. A schematic representation of the reactor is presented in Fig. 1. The MS is a Pfeiffer OmniStar 320 with a Faraday and secondary electron detector (MS-SED) For the gas analysis, a specifically developed calculation routine within MATLAB R2016b was used to quantify the partial pressures as a function of the reaction temperature starting from the raw data (Mutschler et al., 2018a).

2.3. Performance tests for methanation

Prior to methanation experiments, the catalysts were preconditioned. First, the reactor and the piping were preheated at 150 °C in He flow to evaporate the moisture. Second, the catalyst was reduced in H_2 to eliminate the oxygenated species from the samples. This operation was made by feeding 15 mL of H_2 and 5 mL of He at a temperature ranging from 150 to 450 °C. The temperature ramp was 2 °C/min. During this operation, only water and methane were detected as products.

After catalyst reduction, the CO_2 methanation experiments were performed. A gas mixture of CH_4:CO_2:H_2 was used. Unless differently specified, the stoichiometric ratio was 1:1:4 and the flow rates were 1.67, 1.67 and 6.68 mL/min, respectively. The amount of catalyst in every reactor was 258 mg for Ni and 308 mg for Ru/Al_2O_3 (six pellets). For each experiment, one reactor at a time underwent a temperature ramp from 200 to 550 °C at

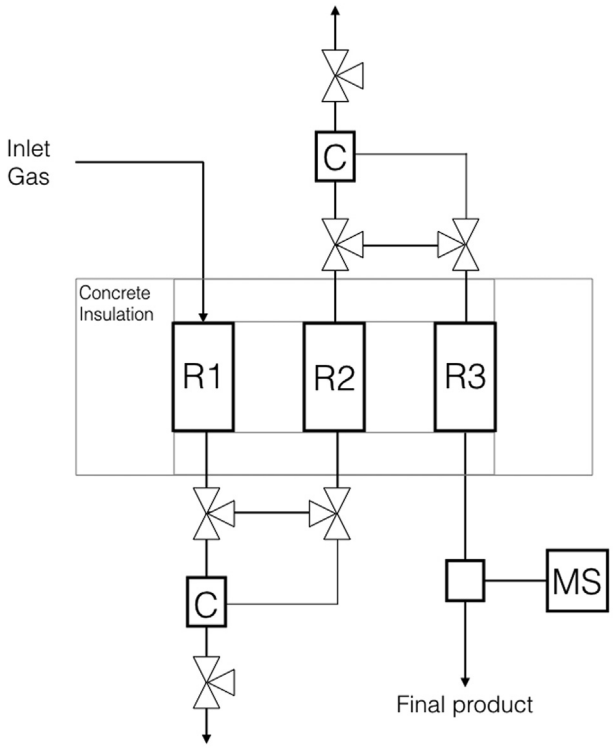

Fig. 1. Scheme of the set-up used. Explanation of symbols: Rn = reactors; C = condenser; MS = mass spectrometer.

2 °C/min, while the other reactors were kept at a constant temperature.

The performance of the reactors is determined by CO_2 conversion:

$$X_{CO_2} = \frac{p_{products}}{p_{products} + p_{CO_2,outlet}} \quad (4)$$

p_i is the partial pressure of the specified component.

Methane yield is calculated as:

$$Y_{CH_4} = X_{CO_2} * \frac{p_{CH_4}}{p_{products}} \quad (5)$$

The yield to CO is given by:

$$Y_{CH_4} = X_{CO_2} - Y_{CH_4} \quad (6)$$

2.4. Thermodynamic equilibrium calculation

The thermodynamic equilibrium is calculated according to the 'extent of reaction' method. To determine the concentration of all the species involved, reactions (1) and (2) must be considered. The ideal gases state equation is used. The two equilibrium relationships are written as:

$$K_{eq,Sab} = \frac{p_{CH_4} p_{H_2O}^2}{p_{CO2} p_{H_2}^4} \quad (7)$$

$$K_{eq,RWGS} = \frac{p_{CO} p_{H_2O}}{p_{CO2} p_{H_2}} \quad (8)$$

The equilibrium constants are calculated from the van't Hoff equation:

$$\ln(K_{eq}) = -\frac{\Delta G_R(T)}{RT} = -\frac{\Delta H_R(T)}{RT} + \frac{\Delta S_R(T)}{R} \quad (9)$$

The reaction enthalpy and entropy are calculated according to the NIST chemistry WebBook (Burgess, 2018).

3. Results and discussion

3.1. Thermodynamics

To set the framework of the analysis, an appropriate thermodynamic study is necessary. The equilibrium concentrations of the species involved in the process (CO_2, CO, CH_4, H_2 and H_2O) are calculated according to the model explained in Section 2.4. The CO_2 conversion and CO yield at equilibrium as a function of temperature for various CH_4:CO_2 ratios, at constant CO_2:H_2 = 1:4 ratio, are displayed in Fig. 2. The results are calculated at atmospheric pressure because most of the experiments of this work are performed at this pressure. We can observe that, for a CH_4:CO_2 ratio of 1, the yield of CO is negligible below 400 °C. In the same conditions, the maximum temperature to achieve CO_2 conversion above 96% is 275 °C. Even though CH_4 and CO_2 are in the optimal stoichiometric ratio for the dry reforming reaction, this does not contribute to the CO_2 conversion, as the equilibrium constant value is extremely low and a large amount of H_2 is present in the reactive mixture. The CH_4:CO_2 ratio is an important parameter to consider for the upgrading of biogas because it can change according to the origin of the biogas and the operating conditions of the digester. The increase in CH_4 content at the inlet of the reactor causes a decrease in the conversion and an increase in the selectivity to CO. This is evident in the graph of CO yield, where we can notice that CO is first formed at a lower temperature for higher CH_4:CO_2 ratio. This is an expected result because CH_4 is a product of the Sabatier reaction and its presence causes a decrease in the extent of advancement of this reaction, leaving more CO_2 available for the RWGS reaction. If higher CO_2 conversion is desired, the thermodynamic limit can be raised by increasing the pressure. As an example, the curves for 1 and 2 bar are reported in the supplementary information (Fig. S1). At 2 bar, the temperature for CO_2 conversion above 96% is 290 °C.

3.2. Optimal temperature profile

3.2.1. Ru-based catalyst

The first experimental series was performed with the state-of-the-art 0.5% Ru/Al_2O_3 catalyst loaded in all three reactors. This catalyst configuration is chosen to create a benchmark to be compared with the following experiments. The experimental procedure is as follows: CH_4, CO_2 and H_2 are fed at atmospheric pressure at the first reactor in a 4:1:1 ratio. A total gas flow of 10 mL/min is applied. Initially, a temperature ramp of 2 °C/min is set in the first reactor, while the second and third are in stand-by, at 150 °C. This temperature is selected to avoid condensation of the water produced in the reaction and to keep the reactors below the catalyst activation temperature. According to the results of this first ramp, the temperature in the first reactor is set at the optimal value (in terms of CO_2 conversion) and the procedure is repeated with the second reactor. In this way, it is possible to find the optimal temperature in the second reactor, with the third reactor in stand-by. As a final step, the first and second reactors are operated at the respective optimal temperatures and the temperature ramp is performed in the third reactor. With this series of experiments, the optimal temperature profile in the three reactors

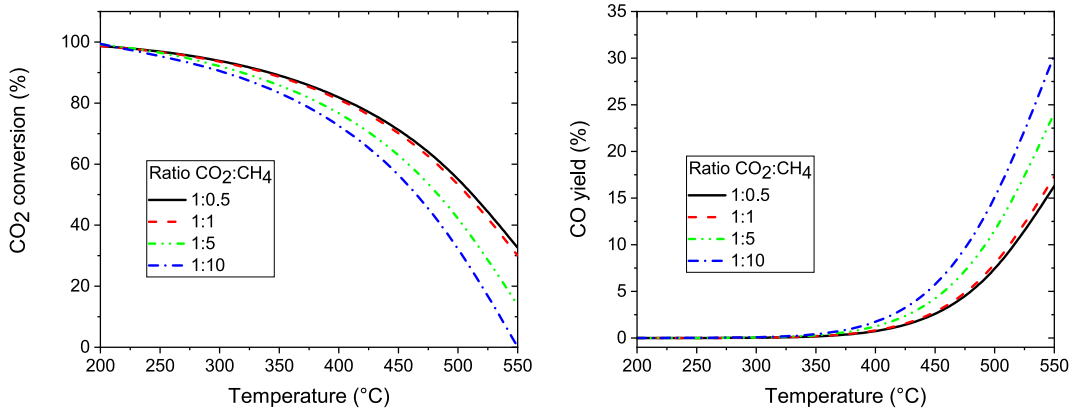

Fig. 2. The equilibrium CO_2 conversion and CO yield at various CO_2:CH_4 ratios at the reactor inlet (P = 1 bar, CO_2:H_2 = 1:4).

is elucidated. The three curves of CO_2 conversion vs. temperature are reported in Fig. 3. The Ru/Al_2O_3 catalyst is highly active in the Sabatier reaction, and a significant CO_2 conversion (ca. 15%) is obtained already at 300 °C. The maximum in the conversion curve for the first reactor is found at 390 °C and it corresponds to 86%. Above this temperature, the conversion curve overlaps with the thermodynamic equilibrium. The curve obtained for the second reactor starts at 86% conversion, the optimal value of the first step, and shows a slight increase with temperature. The highest conversion (90%) is reached at 360 °C, corresponding to the thermodynamic equilibrium value at this temperature. The curve recorded in the third reactor shows a limited increase in the CO_2 conversion with temperature. However, the additional CO_2 conversion added by this last reactor at the optimal point corresponds to only 2%, resulting in a total conversion of 92%. These results confirm the well-known design practice for equilibrium exothermic reactions, which requires that the reactor temperature is decreased with increasing conversion (Moioli et al, 2019a). In this specific case, each reactor is operated at the same space velocity (SV = 2 L/(h g_{cat})). Thus, we demonstrated that, in these conditions, each additional step shifts the maximum to approximatively 20 °C lower temperature and consequently to a higher conversion value according to the thermodynamic equilibrium curve. The reactor system performance can be enhanced by decreasing the SV step after step, to compensate for the lower reaction rate.

Because the optimum of the first reactor lies at high temperature, this reactor can be operated also on a less active catalyst. We selected pristine Ni as a comparison catalyst, to underline the effect of using a catalyst with low activity in the initial stage of the process.

3.2.1.1. Hybrid reactor: Ni followed by Ru-based catalyst. Fig. 4 shows the CO_2 conversion vs. temperature curves for the three reactors filled with pristine Ni (first stage) and Ru/Al_2O_3 (second and third stages). The results are significantly different from the single Ru/Al_2O_3 case (Fig. 3). In this case, the reaction activates at a higher temperature on the first reactor, with the consequence that the maximum CO_2 conversion value is found at a higher temperature that is 42% at 550 °C. As in the previous case, the maximum corresponds to the thermodynamic equilibrium. The curve is not continued after reaching the thermodynamic equilibrium to avoid catalyst deactivation. When the product mixture of the first reactor is fed to the second reactor, no increase in the CO_2 conversion is observed between 200 and 250 °C. Afterwards, CO_2 conversion increases with temperature, until reaching a maximum at 370 °C and 88% conversion. The third reactor increases the conversion by an additional 3%, reaching the maximum at 350 °C and 92% conversion. Hence, the overall performance of the system is maintained constant by the substitution of Ru/Al_2O_3 with Ni in the first reactor. The origin of this change can be explained by complementing the CO_2 conversion results with the corresponding graphs of CO and CH_4 yields. These additional profiles are reported in Fig. 5 for the 1st and 2nd steps.

For the Ni-filled reactor, the CO_2 conversion and the CH_4 yield are overlapping below 450 °C because in this region the CO yield is negligible. Above this temperature, the formation of CO is significant, with an increasing trend with temperature, which follows the thermodynamic equilibrium curve. At 550 °C, all three components reach thermodynamic equilibrium. When the gas mixture produced in the first reactor is fed to the second reactor, we can observe that the presence of CO significantly modifies the reactivity compared with the case of Section 3.2.1. At first, the reaction taking place is the CO methanation, leading to CH_4 formation. This reaction is observed at a lower temperature than the Sabatier reaction and leads to the complete consumption of the CO at 250 °C. In this region, no CO_2 conversion is observed, which is in line with the results of Section 3.2.1. As a consequence, CO_2 conversion and CH_4 yield start to overlap at 250 °C. At higher temperature, the Sabatier reaction takes place on the Ru/Al_2O_3 and CO_2 conversion and CH_4 yield grow contemporaneously until reaching the thermodynamic equilibrium curve above 370 °C. In this way, we confirm that the CO is a key intermediate of the CO_2 methanation because this latter reaction can occur only when CO is completely consumed (Zhao et al., 2018). The different performance of the hybrid configuration compared with the 'Ru-only' configuration is thus originated by the peculiar role of CO. Because the CO methanation is faster than the Sabatier reaction, the presence of a mixture of CO_2 and CO at the reactor inlet reduces the residence time required to reach the

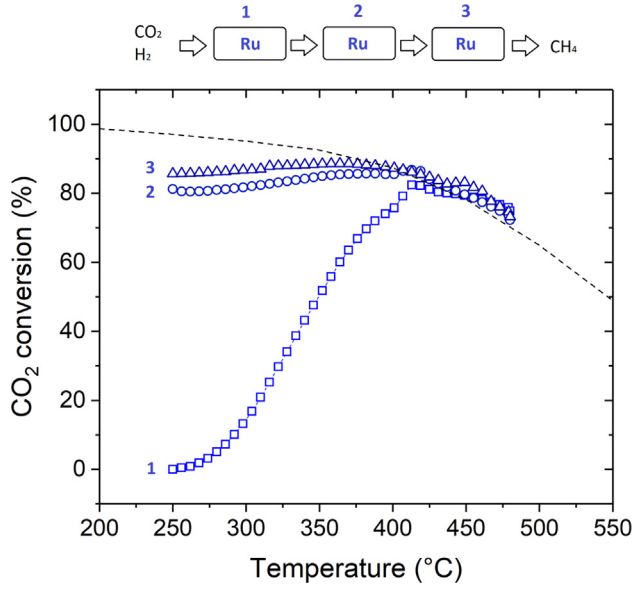

Fig. 3. CO_2 conversion vs. temperature over the 0.5% Ru/Al_2O_3 catalyst. The optimal temperature is 390 °C for the first reactor, 350 °C for the second and 330 °C for the third (□ 1st step, ○ after 2 steps, △ after 3 steps; — thermodynamic equilibrium).

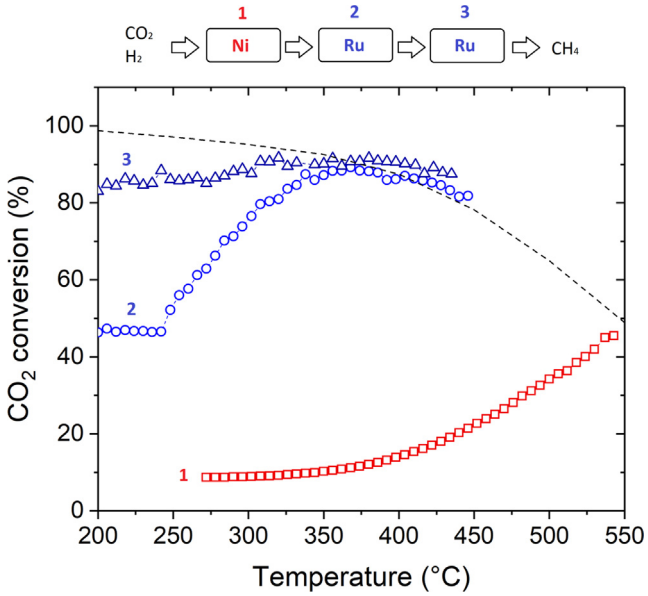

Fig. 4. CO_2 conversion vs. temperature over a first Ni catalyst followed by two steps over the 0.5% Ru/Al_2O_3 catalyst. The optimal temperature is 550 °C for the first reactor, 360 °C for the second, 330 °C for the third. (red: Ni, blue: Ru/Al_2O_3 catalyst; □ 1st step, ○ after 2 steps, △ after 3 steps; — thermodynamic equilibrium).

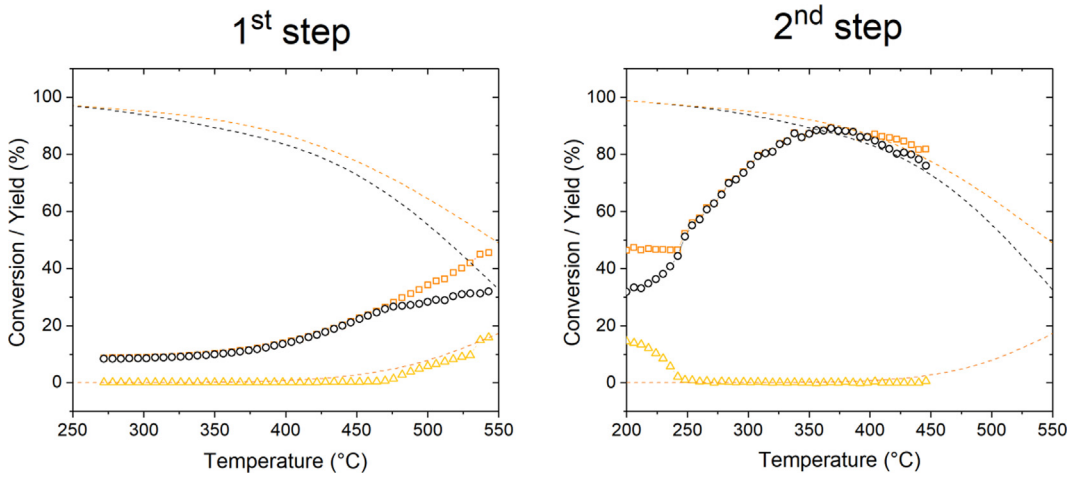

Fig. 5. CO_2 conversion, CH_4 and CO yield vs. temperature in the first and second steps of the hybrid reactor (□ CO_2 conversion, ○ CH_4 yield, △ CO yield, — thermodynamic equilibrium, following the colour code for CO_2, CH_4 and CO).

desired CO_2 conversion (Falbo et al., 2019). This allows reaching the thermodynamic equilibrium curve at a lower temperature and thus at a higher conversion value. The results of these two steps can be seen as representative of a single hybrid-bed Sabatier reactor, where first high temperature is reached in the hotspot over Ni and then the reaction is continued over Ru/Al_2O_3 after quick cooling to the final temperature. The activity in the CO methanation is the key for the performance improvement when using a 'hybrid-bed' reactor. As a comparison, we observed that, when also the second catalyst bed is Ni, the function of this second step is limited. In fact, as observable in Fig. S2, this catalyst shows low activity in the CO methanation, so that the CO concentration remains almost constant until 400 °C. Above this temperature, the concentration decreases, until reaching thermodynamic equilibrium. However, above 400 °C also the Sabatier reaction is active, resulting in an increase of the CO_2 conversion, limited to an additional 10%.

The multistep Sabatier reactor concept could be further enhanced by operating the second step with a tailored Ni catalyst with higher performance (e.g. (Garbarino et al., 2019; Guerra et al., 2018; Koschany et al., 2016; Vrijburg et al., 2019)), employing a limited amount of the Ru-based catalyst only in the final step.

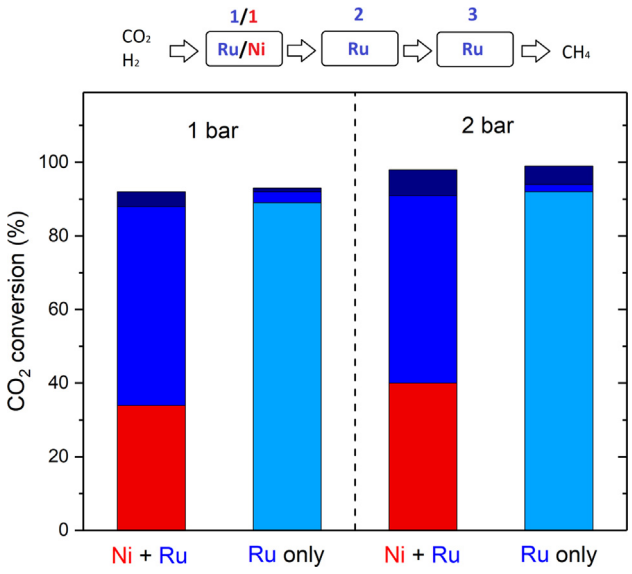

Fig. 6. Effect of pressure on the CO_2 conversion value: the increase to 2 bar increases the CO_2 conversion to a value above 99% (red: Ni, blue: 0.5% Ru/Al_2O_3 catalyst).

3.3. Effect of pressure

As observed in the previous section, the maximum CO_2 conversion reachable in the reactors is determined by the match of kinetics and thermodynamics. The former can be modified by changing the catalyst or operating on the SV, while the latter can be altered only by modifying the pressure (at constant stoichiometric ratio). To determine the influence of higher pressure, the experiments of Section 2 were repeated at 2 bar. The results showing the maximum CO_2 conversion in the three stages are reported in Fig. 6. For the 'Ru-only' system, the increase of conversion in the first two stages is moderate, reaching the values of 92 and 94%, respectively (compared with 88 and 90% of the 1 bar experiments). The conversion increase in the third step is important, leading to a CO_2 concentration in the outlet gas below the detectability threshold of the MS spectrometer. This corresponds to an extremely high conversion value, quantifiable as > 99%. The improvement in the CO_2 conversion originates from the combined effect of pressure on thermodynamics and kinetics. In fact, even though the effect of pressure on kinetics is generally limited and originates from the higher concentration of the gas, when the CO_2 conversion is high (i.e. > 90%), the increase in pressure results in an important relative increase of the reaction rate. The key to the improved performance at 2 bars is hence the shift towards higher temperature in the driving force generated by the thermodynamic equilibrium, which reduces the influence of the reverse reaction.

The influence of pressure is important also in the 'hybrid-bed' case. In this reactor configuration, the increase of pressure involves also the change of RWGS equilibrium. In fact, as underlined in Section 3.1, the increase of pressure shifts the equilibrium of CO formation towards higher temperature. For this reason, we observe an increase in the CO_2 conversion in the first reactor stage (over Ni): in fact, the production of CO is low and CO_2 conversion and CH_4 yield coincide. This is shown in Fig. S3. However, the absence of CO at the outlet gas of the first reactor has a negative impact on the second reactor: it brings the conversion from 88% up to 90% (+2%), while in the 1 bar case the increase in conversion corresponds to 6%. Here, we observe a different reaction than for the similar case of Section 3.2, where we underlined the higher reaction rate of CO methanation compared with the Sabatier reaction.

In this case, the absence of CO causes an increase in the residence time required for the reaction, causing the decrease of outlet conversion at constant SV. Despite this, as in the 'Ru-only' case, the third reactor completes the reaction, reaching a global CO_2 conversion value above 99%.

In conclusion, with the reactive system presented in this paper, it is possible to reach a CO_2 conversion compatible with the grid injection with a SV of 2 L/(h g_{cat}) at 2 bar. Additionally, with the temperature control strategy employed here, it is possible to limit the deactivation phenomena on the Ni catalyst, as the maximal operating temperature of 550 ℃ is not overcome. This was evident in the experimental campaign, as no deactivation of the catalyst was observed over time and the results of the reference experiment were always confidently reproduced.

3.4. Effect of space velocity

The SV is the main factor determining the performance of the reactor. In the previous sections, SV was kept constant at 2 L/(h g_{cat}) for every reactor, to highlight the effect of the manipulation of the temperature profile on the CO_2 conversion. Here, we discuss the effect of varying the SV on the CO_2 conversion in the reactor loaded with the 0.5% Ru/Al_2O_3 catalyst in every step. This system has been chosen to minimize the observation of effects related to the presence of side reactions and only focus on the Sabatier reaction. Fig. 7 shows the CO_2 conversion recorded at different global values of SV, while keeping the optimal temperatures found previously for each step (in order, 380, 350 and 330 °C). The amount of catalyst is constant in the three reactors so that the total SV is simply one-third of the SV of each reactor, i.e. 0.67 L/(h g_{cat}). The reference point, obtained in Section 3.2, shows a CO_2 conversion of 92%. This point is already close to the thermodynamic limit for the temperature of the 3rd reactor (ca. 300 °C). For this reason, we observe that a decrease of the SV has a limited influence on the total conversion, reaching the equilibrium value already at SV of 0.5 L/(h g_{cat}). An increase in SV from the reference point has instead an important influence on the conversion because at 1 L/(h g_{cat}) it is reduced to 89% and at 1.3 L/(h g_{cat}) to 86%. From a process point of view, SV should be selected at the minimum value that allows reaching the thermodynamic equilibrium, in order to obtain the required conversion with the minimal size of the reactor.

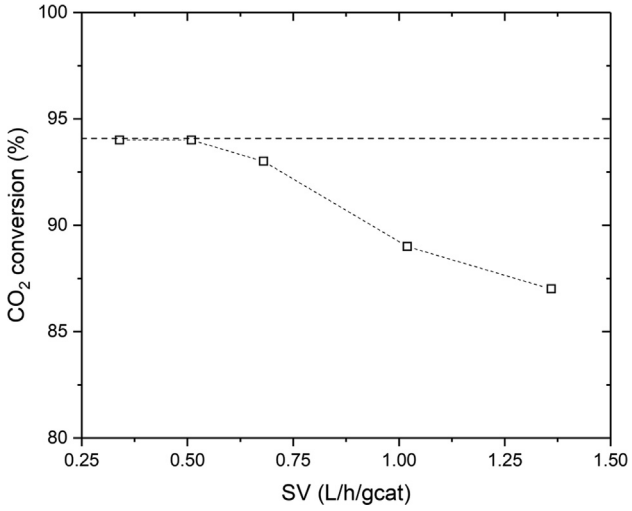

Fig. 7. Effect of space velocity on CO_2 conversion (– thermodynamic equilibrium, temperature of the 3rd stage: 300 °C).

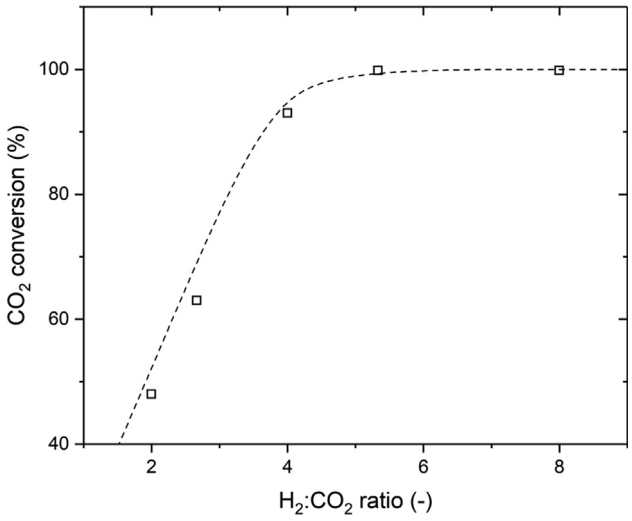

Fig. 8. Effect of the inlet $H_2:CO_2$ ratio on the CO_2 conversion (– thermodynamic equilibrium, $CH_4:CO_2$ = 1, total SV = 1.67 L/(h g_{cat})).

3.5. Effect of the stoichiometric ratio

The study of the effect of the stoichiometric ratio is an important point in the analysis of the biogas upgrading because the relative amounts of CO_2 and CH_4 may vary according to the conditions in the biogas production. As a first comparison, we analysed the effect of the $H_2:CO_2$ ratio. A variation in this parameter can be seen as the consequence of a sudden change in the biogas composition, not compensated by an adaptation of the H_2 fed to the reactor. The results of the experiments at various $H_2:CO_2$ values are shown in Fig. 8. Starting from the design point, at $H_2:CO_2$ = 4, we can observe how the CO_2 conversion is modified by increasing or decreasing this ratio, in relation to the thermodynamic equilibrium. At hydrogen-rich conditions ($H_2:CO_2$ > 4), the CO_2 conversion increases, as expected according to the thermodynamic equilibrium. All the points collected in this region lie directly on the equilibrium line, showing the important influence of the thermodynamic limit on the reaction rate. At $H_2:CO_2$ > 5, full CO_2 conversion is reached. However, the resulting gas will be outside the gas grid injection specifications because the composition of the gas after condensation at $H_2:CO_2$ = 5 and full conversion results as 50% CH_4 and 50% H_2. When the reactor is operated in hydrogen-lean conditions, the CO_2 conversion points are more distant from the thermodynamic equilibrium, suggesting an inhibiting effect of the CO_2 excess on the reaction kinetics. Apart from the mechanistic considerations, the excess/defect of reactants should be evaluated under a process perspective, as the remaining reactants must be further treated to reach the grid injection regulations. In this sense, the reactor and the downstream processing should be carefully integrated and optimized as inter-dependent units.

The influence of the $CH_4:CO_2$ ratio is more difficult to forecast because this parameter significantly influences both the thermodynamics and the kinetics of the reaction. Starting from the design point at $CH_4:CO_2$ = 1 and 92% conversion, in Fig. 9 we observe that an increase in the methane content in the reactants increases the CO_2 conversion, even though this slightly decreases the equilibrium conversion. The reason for this phenomenon is the decrease in the 'real' SV because the amount of gas is kept constant, but the fraction of reactive gas is decreased. Furthermore, at low concentration of the reactants, the amount of water produced is limited, avoiding the inhibiting effect of water on reaction kinetics (Wang et al., 2016). Additionally, with large amount of methane, the reaction hotspot is reduced, due to the dilution effect, decreasing the need for rapid cooling to complete the reaction. On the other side, the decrease in the

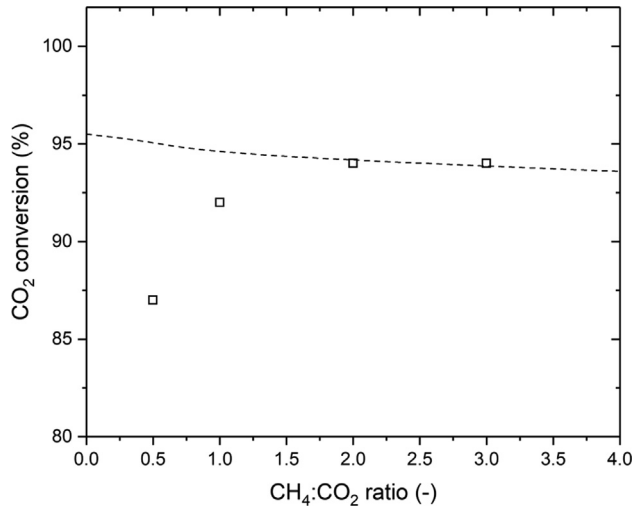

Fig. 9. Effect of the inlet CH_4:CO_2 ratio on the CO_2 conversion (– thermodynamic equilibrium, H_2:CO_2 = 4, total SV = 1.67 L/(h g_{cat})).

methane contents causes an increase in the 'real' SV, decreasing the CO_2 conversion. For this reason, at CH_4:CO_2 = 0.5, we measured the lowest CO_2 conversion, 85%.

These experiments demonstrate the important influence of the gas composition on the optimal temperature profile in the reactor. The various parameters, apparenly independent, are in reality inter-dependent and influence the performance of the biogas upgrading under both a reactor and process optimization perspective. For this reason, the temperature profile in the reactor must be adapted during dynamic operation according to the quality of the biogas. However, a full description of this type of dynamic operation is beyond the scope of this paper and this topic will be investigated in future work of the group.

4. Conclusions

In this paper, we presented the results of CO_2 methanation tests performed with a new system composed of three consecutive reactors used for synthetic natural gas production from biogas. The set-up allows the free manipulation of the temperature in the three steps and the determination of the optimal temperature profile to maximize the CO_2 conversion in different conditions. When the reactor is operated with a 0.5% Ru/Al_2O_3 catalyst, 92% CO_2 conversion is achieved with a SV of 2 L/(h g_{cat}) per stage and at a pressure of 1 bar. In this case the temperatures of the three stages are 390, 350 and 330 °C, respectively. Ni, a cheaper but worse performing catalyst, can replace Ru/Al_2O_3 in the first stage with the result that the optimal temperature in this stage is increased to the maximum temperature allowed, that is 550 °C. At this temperature, the contribution of the RWGS reaction is important and a significant amount of CO is found at the outlet of the first reactor. This CO is then converted in the second step in the CO methanation reaction, which is faster than the Sabatier reaction. For this reason, the activation temperature of the second reactor is significantly lower than in the Ru/Al_2O_3-only case. Hence, by introducing Ni in the first stage, we can still achieve 92% conversion, but with a lower amount of noble metal catalyst. The CO_2 conversion can be further increased by increasing the pressure of the system. We observed that in both reactor configurations a CO_2 conversion above 99.5% can be achieved already at 2 bar.

We thus demonstrated that the methanation of the CO_2 present in biogas can be an effective strategy for upgrading this resource and that this can be achieved with high efficiency in a simple system, just by tailoring the temperature profile to the properties of the feed gas. This allows a flexible operation of the biogas upgrading, opening the way for an effective sector coupling between renewable gas production and storage of excess electrical energy.

CRediT authorship contribution statement

Emanuele Moioli: Conceptualization, Methodology, Formal analysis, Data curation, Writing - original draft, Writing - review & editing. **Robin Mutschler:** Investigation, Formal analysis, Writing - original draft. **Alexandre Borsay:** Investigation, Formal analysis, Writing - original draft. **Marco Calizzi:** Formal analysis, Writing - original draft. **Andreas Züttel:** Resources, Supervision, Funding acquisition.

Declaration of Competing Interest

The authors declared that there is no conflict of interest.

Acknowledgements

The collaboration with Gaznat and the financial support by the KTI/CTI (now Innosuisse), project no. 6441.1 PFIW-IW are gratefully acknowledged. The authors thank EPFL Library for the support to publish open access.

Appendix A. Supplementary material

Supplementary data to this article can be found online at https://doi.org/10.1016/j.cesx.2020.100078.

References

De Saint Jean, M., Baurens, P., Bouallou, C., Couturier, K., 2015. Economic assessment of a power-to-substitute-natural-gas process including high-temperature steam electrolysis. Int. J. Hydrogen Energy 40, 6487–6500. https://doi.org/10.1016/j.ijhydene.2015.03.066.

Burgess, D.R., 2018. Thermochemical Data, in "NIST Chemistry WebBook". National Institute of Standards and Technology, Gaithersburg MD.

El Sibai, A., Rihko Struckmann, L.K., Sundmacher, K., 2017. Model-based Optimal Sabatier Reactor Design for Power-to-Gas Applications. Energy Technol. 5, 911–921. https://doi.org/10.1002/ente.201600600.

Falbo, L., Martinelli, M., Visconti, C.G., Lietti, L., Bassano, C., Deiana, P., 2018. Kinetics of CO2methanation on a Ru-based catalyst at process conditions relevant for Power-to-Gas applications. Appl. Catal. B Environ. 225, 354–363. https://doi.org/10.1016/j.apcatb.2017.11.066.

Falbo, L., Visconti, C.G., Lietti, L., Szanyi, J., 2019. The effect of CO on CO2 methanation over Ru/Al2O3 catalysts: a combined steady-state reactivity and transient DRIFT spectroscopy study. Appl. Catal. B Environ. 117791. https://doi.org/10.1016/j.apcatb.2019.117791.

Fukuhara, C., Hayakawa, K., Suzuki, Y., Kawasaki, W., Watanabe, R., 2017. A novel nickel-based structured catalyst for CO2methanation: A honeycomb-type Ni/CeO2catalyst to transform greenhouse gas into useful resources. Appl. Catal. A Gen. 532, 12–18. https://doi.org/10.1016/j.apcata.2016.11.036.

Gallandat, N., Mutschler, R., Vernay, V., Yang, H., Züttel, A., 2018. Experimental performance investigation of a 2 kW methanation reactor. Sustain. Energy Fuels 2, 1101–1110. https://doi.org/10.1039/C8SE00073E.

Garbarino, G., Wang, C., Cavattoni, T., Finocchio, E., Riani, P., Flytzani-Stephanopoulos, M., Busca, G., 2019. A study of Ni/La-Al 2 O 3 catalysts: A competitive system for CO 2 methanation. Appl. Catal. B Environ. 248, 286–297. https://doi.org/10.1016/j.apcatb.2018.12.063.

Götz, M., Lefebvre, J., Mörs, F., McDaniel Koch, A., Graf, F., Bajohr, S., Reimert, R., Kolb, T., 2016. Renewable Power-to-Gas: A technological and economic review. Renew. Energy. https://doi.org/10.1016/j.renene.2015.07.066

Guerra, L., Rossi, S., Rodrigues, J., Gomes, J., Puna, J., Santos, M.T., 2018. Methane production by a combined Sabatier reaction/water electrolysis process. J. Environ. Chem. Eng. 6, 671–676. https://doi.org/10.1016/j.jece.2017.12.066.

Jürgensen, L., Ehimen, E.A., Born, J., Holm-Nielsen, J.B., 2015. Dynamic biogas upgrading based on the Sabatier process: Thermodynamic and dynamic process simulation. Bioresour. Technol. 178, 323–329. https://doi.org/10.1016/j.biortech.2014.10.069.

Jürgensen, L., Ehimen, E.A., Born, J., Holm-Nielsen, J.B., 2014. Utilization of surplus electricity from wind power for dynamic biogas upgrading: Northern Germany

case study. Biomass Bioenergy 66, 126–132. https://doi.org/10.1016/j.biombioe.2014.02.032.
Kapoor R, Ghosh P, Kumar M, Vijay VK. Evaluation of biogas upgrading technologies and future perspectives : a review. Env Sci Pollut Res 2019, 26, 11631-11661. https://doi.org/https://doi.org/10.1007/s11356-019-04767-1.
Kiewidt, L., Thöming, J., 2015. Predicting optimal temperature profiles in single-stage fixed-bed reactors for CO2-methanation. Chem. Eng. Sci. 132, 59–71. https://doi.org/10.1016/j.ces.2015.03.068.
Koschany, F., Schlereth, D., Hinrichsen, O., 2016. On the kinetics of the methanation of carbon dioxide on coprecipitated NiAl (O) x. Appl. Catal. B, Environ. 181, 504–516. https://doi.org/10.1016/j.apcatb.2015.07.026.
Moioli, E., Gallandat, N., Züttel, A., 2019a. Model based determination of the optimal reactor concept for Sabatier reaction in small-scale applications over Ru/Al2O3. Chem. Eng. J. 375,. https://doi.org/10.1016/j.cej.2019.121954 121954.
Moioli, E., Gallandat, N., Züttel, A., 2019b. Parametric sensitivity in the Sabatier reaction over Ru/Al2O3 – theoretical determination of the minimal requirements for reactor activation. React. Chem. Eng. 4, 100–111. https://doi.org/10.1039/C8RE00133B.
Moioli, E., Züttel, A., 2020. A model-based comparison of Ru and Ni catalysts for the Sabatier reaction. Sustain. Energy Fuels 4, 1396–1408. https://doi.org/10.1039/c9se00787c.
Mutschler, R., Luo, W., Moioli, E., Züttel, A., 2018a. Fast real time and quantitative gas analysis method for the investigatiin of the CO2 reduction reaction mechanism. Rev. Sci. Instrum. 89. https://doi.org/10.1063/1.5047402.
Mutschler, R., Moioli, E., Luo, W., Gallandat, N., Züttel, A., 2018b. CO2hydrogenation reaction over pristine Fe Co, Ni, Cu and Al2O3supported Ru: Comparison and determination of the activation energies. J. Catal. 366, 139–149. https://doi.org/10.1016/j.jcat.2018.08.002.
Mutschler, R., Moioli, E., Züttel, A., 2019. Modelling the CO2 hydrogenation reaction over Co, Ni and Ru/Al2O3. J. Catal. 375, 193–201. https://doi.org/10.1016/j.jcat.2019.05.023.
Schaaf, T., Grünig, J., Schuster, M.R., Rothenfluh, T., Orth, A., 2014. Methanation of CO2- storage of renewable energy in a gas distribution system. Energy. Sustain. Soc. 4, 1–14. https://doi.org/10.1186/s13705-014-0029-1.
Schweizerischer Verein des Gas- und Wasserfaches SVGW/SSIGE, 2014. Réglementation G13: Directive pour l'injection de biogaz 2008, 33.
Schweizerischer Verein des Gas- und Wasserfaches SVGW/SSIGE, 2013. Réglementation G18: Directive pour la qualité du gaz.
Vrijburg, W.L., Moioli, E., Chen, W., Zhang, M., Terlingen, B., Zijlstra, B., Filot, I.A.W., Zuttel, A., Pidko, E.A., Hensen, E.J.M., 2019. An Efficient Base-Metal NiMn/TiO2 Catalyst for CO2 Methanation. ACS Catal. acscatal.9b01968. https://doi.org/10.1021/acscatal.9b01968.
Wang, X., Hong, Y., Shi, H., Szanyi, J., 2016. Kinetic modeling and transient DRIFTS–MS studies of CO2methanation over Ru/Al2O3catalysts. J. Catal. 343, 185–195. https://doi.org/10.1016/j.jcat.2016.02.001.
Witte, J., Calbry-Muzyka, A., Wieseler, T., Hottinger, P., Biollaz, S.M.A., Schildhauer, T.J., 2019. Demonstrating direct methanation of real biogas in a fluidised bed reactor. Appl. Energy 240, 359–371. https://doi.org/10.1016/j.apenergy.2019.01.230.
Witte, J., Settino, J., Biollaz, S.M.A., Schildhauer, T.J., 2018a. Direct catalytic methanation of biogas – Part I: New insights into biomethane production using rate-based modelling and detailed process analysis. Energy Convers. Manag. 171, 750–768. https://doi.org/10.1016/j.enconman.2018.05.056.
Witte, J., Settino, J., Biollaz, S.M.A., Schildhauer, T.J., 2018b. Direct catalytic methanation of biogas – Part II: Techno-economic process assessment and feasibility reflections. Energy Convers. Manag. 178, 26–43. https://doi.org/10.1016/j.enconman.2018.05.056.
Zhao, K., Wang, L., Calizzi, M., Moioli, E., Zuttel, A., 2018. In situ Control of the Adsorption Species in CO 2 Hydrogenation: Determination of Intermediates and Byproducts. J. Phys. Chem. C 122, 20888–20893. https://doi.org/10.1021/acs.jpcc.8b06508.